Journal of Catalysis 284 (2011) 90–101

Contents lists available at SciVerse ScienceDirect

Journal of Catalysis

journal homepage: www.elsevier.com/locate/jcat

Selective conversion of furfural to methylfuran over silica-supported Ni—Fe bimetallic catalysts

Surapas Sitthisa, Wei An, Daniel E. Resasco *

School of Chemical, Biological and Materials Engineering and Center for Biomass Refining, University of Oklahoma, Norman, OK 73019, USA

ARTICLE INFO

Article history:
Received 14 July 2011
Revised 2 September 2011
Accepted 6 September 2011
Available online 7 October 2011

Keywords:
Furfural
Furfuryl alcohol
Methylfuran
Ni—Fe alloys
Hydrogenolysis
Hydrogenation
Decarbonylation
Bio-oil upgrading

ABSTRACT

The conversion of furfural in H_2 over SiO_2-supported Ni and Ni—Fe bimetallic catalysts has been investigated at 1 bar in the 210–250 °C temperature range. Over the monometallic Ni catalyst, furfuryl alcohol and furan are primary products resulting from hydrogenation and decarbonylation, respectively. These primary products are further converted in secondary reactions. Furan yields C_4 products (butanal, butanol, and butane) via ring opening, while furfuryl alcohol produces 2-methylfuran via C—O hydrogenolysis. By contrast, 2-methylfuran is not produced to a great extent on pure Ni at any level of overall conversion. But, on Fe—Ni bimetallic catalysts, the yield of 2-methylfuran greatly increases while the yields of furan and C_4 products decrease. That is, the addition of Fe suppresses the decarbonylation activity of Ni while promoting the C=O hydrogenation (at low temperatures) and the C—O hydrogenolysis (at high temperatures). DFT analysis of the possible surface species on the mono- and bimetallic surfaces suggests that the differences in selectivity displayed by these catalysts can be attributed to the stability of the η^2-(C,O) surface species, which is higher on the Ni—Fe than on pure Ni. As a result, this η^2-(C,O) species can be readily hydrogenated to furfuryl alcohol and subsequently hydrogenolyzed to 2-methylfuran on the bimetallic alloy due to a strong interaction between the carbonyl O and the oxyphilic Fe atoms. Without Fe, on the pure Ni surface, the η^2-(C,O) species can be converted into a surface acyl species, which can be decomposed to produce furan and CO. Detailed XRD and TPR characterization indicate the formation of Fe—Ni alloys in all the bimetallic catalysts.

1. Introduction

Furfurals are a family of aromatic compounds produced from the dehydration of sugars and are major components of bio-oil [1,2]. Due to their high reactivity, these compounds require further upgrading to more stable products if the goal is to incorporate them to the gasoline/diesel pool. Several approaches for furfural conversion have been attempted. Aldol condensation of furfural with small ketones is a promising approach to produce larger compounds (C_8—C_{15}) that may fall in the fuel range [3–6]. High yields of condensation products by direct condensation of furfural with acetone have been obtained in the presence of basic catalysts. However, condensation is only the first step. Selective deoxygenation is necessary to obtain compounds acceptable as components of transportation fuels. A highly desirable outcome of this deoxygenation step is preserving C—C bonds while effectively breaking the C—O bonds. Therefore, it is important to investigate what catalysts are effective for this task, how do they operate, and what are the possible reaction pathways.

Metal catalysts appear as promising candidates for the selective removal of oxygen from the carbonyl group of furfural under relatively mild operating conditions. We have recently shown that different metals exhibit very different product distributions depending on the type and relative stability of the surface species that they are able to form. For example, we recently showed that Cu-based catalysts are highly selective for hydrogenation of furfural to furfuryl alcohol (>95% selectivity) [7]. Microkinetic studies, DFT (Density Functional Theory), and IR spectroscopy have been combined to investigate the nature of the adsorbed species. It was found that the adsorption of furfural on Cu results in an η^1(O)-surface species, in which the carbonyl group is bound to the metal through the O lone pair while the rest of the molecule is pushed away from the surface due to a net repulsion between C and Cu. The preferred adsorption in the η^1(O)-mode is responsible for the high hydrogenation selectivity to furfuryl alcohol, typically observed on Cu-based catalysts [8–10]. By contrast, Group VIII metals (Ni, Pd, and Pt) display a very different behavior. While at low temperatures, they only exhibit hydrogenation activity, with furfuryl alcohol as the major product [11–13], at high temperatures, the decarbonylation reaction dominates, with furan as the main product [14].

* Corresponding author. Tel.: +1 405 325 4370.
E-mail address: resasco@ou.edu (D.E. Resasco).

0021-9517/$ - see front matter © 2011 Elsevier Inc. All rights reserved.
doi:10.1016/j.jcat.2011.09.005

From the point of view of fuel production, neither hydrogenation nor decarbonylation is desirable. While the former does not remove O, the latter loses C in the process. Hydrogenolysis to 2-methylfuran (via C1—O1 hydrogenolysis) would be the most desirable product, since not only has intrinsically good fuel properties (high octane number, RON = 131, low water solubility, 7 g/L [15]) but also can be considered an archetypical product of the desired reaction paths in bio-oil upgrading, i.e., removing O while keeping a high C yield.

Therefore, one of the goals of this study was to find a catalyst that is able to produce 2-methylfuran while suppressing the formation of furan. Our recent study showed that bimetallic alloys can greatly alter the furfural reaction paths. For example, we showed that adding Cu to Pd and forming bimetallic Pd—Cu alloys greatly suppresses the production of furan from furfural. However, only furfuryl alcohol, rather that 2-methylfuran, was observed [16]. In the present work, we have investigated the conversion of furfural over Ni—Fe bimetallic catalysts. The effect of adding Fe on the catalytic properties of silica-supported Ni is investigated. Samples with different Ni/Fe ratios were prepared and characterized by XRD, TEM, TPR, and BET techniques to evaluate the structural changes and the extent of alloy formation. Structure–activity relationships were investigated by combining the results of catalytic activity measurements with characterization and theoretical DFT (Density Functional Theory) calculations.

2. Experimental

2.1. Catalyst synthesis and characterization

The Ni—Fe/SiO_2 catalysts were prepared by incipient wetness co-impregnation, using an aqueous solution containing both metal precursors, $Ni(NO_3)_2{\cdot}6H_2O$ (98%, Alfa Aesar) and $Fe(NO_3)_3{\cdot}9H_2O$ (98% Sigma–Aldrich). Prior to impregnation, the silica support (SiO_2, Hisil 233) was dried overnight at 120 °C. Then, the aqueous solution was added to the support, keeping an incipient wetness liquid/solid ratio of 1 cc/g. The Ni loading was kept constant at 5.0 wt.% on all samples, while the Fe loading was varied from 0.0 to 5.0 wt.%. After impregnation, the catalysts were first dried overnight at room temperature and then placed in an oven at 120 °C for 12 h. The oven-dried catalysts were finally calcined for 4 h at 500 °C, with a linear heating ramp of 10 °C/min, under 100 ml/min flow of pure air. The catalyst powders thus obtained were pressed at 1500 psi, crushed, and sieved to 40–60 mesh.

The reducibility of the calcined samples was determined by temperature programmed reduction (TPR). In these measurements, 20 mg of a sample was placed in a quartz reactor and heated at 30 °C/min up to 500 °C under a He flow of 20 ml/min, and held at this temperature for 1 h. The reactor was then cooled down to 30 °C and the sample exposed to a stream of 5% H_2/Ar at a flow rate of 20 ml/min. Subsequently, the sample was heated up to 800 °C at a heating rate of 5 °C/min. The variation in hydrogen uptake was monitored on a TCD detector as a function of temperature. The molar H_2 uptake per gram of sample was quantified from the peak area in the TPR profiles and calibrated with a CuO standard.

Several physical techniques were employed to characterize the structure of the Ni—Fe/SiO_2 catalysts. X-ray powder diffraction patterns (XRD) for all the samples were collected on a D8 Series II X-ray Diffractometer (BRUKER AXS), using Cu Kα radiation generated at 40 kV and 35 mA. The samples were reduced ex situ under pure H_2 (100 ml/min) at 450 °C for 1 h prior to the measurements. The scans covered the 2θ range from 30° to 60°.

Morphology and size of the Ni—Fe clusters were characterized by transmission electron microscopy (TEM, JEOL model JEM-2100 LaB6). Before TEM analysis, the samples were reduced ex situ in pure H_2 (100 ml/min) at 450 °C for 1 h. The reduced samples were then mixed with 2-propanol, sonicated, deposited onto the TEM (Cu) grids, and dried. The BET surface area (S_g) was measured by conventional N_2 physisorption on a Micromeritics ASAP 2010 unit, after evacuation at 350 °C for 3 h.

2.2. Catalytic activity measurements

The vapor-phase conversion of furfural over the Ni—Fe catalyst series was evaluated in a tubular quartz reactor. In each run, a pelletized catalyst sample (size range: 250–425 μm) was placed at the center of the reactor tube between two layers of glass beads and quartz wool and pre-reduced in H_2 flow (60 ml/min, Airgas, 99.99%) for 1 h at 450 °C. After reduction, the catalyst was cooled down to the selected reaction temperature (210–250 °C) under the same H_2 flow. Prior to the reaction, furfural (Sigma–Aldrich, 99.5%) was purified by vacuum distillation to remove residues and any oligomers formed during storage. The purified liquid was kept under He atmosphere until its use in the reaction test. A 0.5 ml/h (0.006 mol/h) flow of liquid furfural was fed continuously from a syringe pump (Cole Palmer) and vaporized into a H_2 stream of 60 ml/min. The reaction products were analyzed by online GC (Agilent model 6890), using an HP-5 capillary column and a FID detector. The carbon balance was checked in every run and found to be higher than 95% in every case. The product yield and selectivity for each product were calculated as follows:

$$\text{Yield } (\%) = \frac{\text{mol of the product produced}}{\text{mol of furfural fed}} \times 100$$

$$\text{Selectivity } (\%) = \frac{\text{mol of the product produced}}{\text{mol of furfural consumed}} \times 100$$

2.3. Density functional theory calculations

All DFT calculations were performed with the Vienna ab initio simulation package (VASP) [17,18]. A spin-polarized GGA PBE functional [19], all-electron plane-wave basis sets with an energy cutoff of 400 eV, and a projector augmented wave (PAW) method were adopted [20,21]. The Brillouin-zone of the $p(4 \times 4)$ lateral supercell was sampled at $3 \times 3 \times 1$ k-points using the Monkhorst–Pack scheme [21]. First-order Methfessel–Paxton smearing [22] of 0.2 eV was employed in the integration to speed up the convergence. The conjugate gradient algorithm was used in the optimization. The convergence threshold was set to 10^{-4} eV in total energy and 10^{-2} eV/Å in force on each atom. All reported energies are extrapolated to $k_BT = 0$ eV.

The Ni(1 1 1) surface was modeled by a three-layer slab with the bottom two layers fixed at their equilibrium bulk phase positions (calculated lattice constant = 3.522 Å), while the top layer was allowed to relax. The two successive slabs were separated by a 10 Å vacuum region to ensure that the adsorbate (i.e., furfural) and the subsequent slab would not interact. The $p(4 \times 4)$ supercell has a dimension of 9.962 Å × 9.962 Å × 14.068 Å to ensure that the effect of adsorbate–adsorbate interactions between adsorbed furfural molecules is negligible.

The bimetallic NiFe(1 1 1) alloy surface [i.e., $Ni_{0.5}Fe_{0.5}$(1 1 1), subscript is omitted thereafter for simplicity] was cleaved from an optimized NiFe *fcc* unit cell (calculated lattice constant $a = c = 3.553$ Å, $b = 3.582$ Å) [22] and was modeled in the same fashion as the pure Ni(1 1 1) surface. The $p(4 \times 4)$ supercell has a dimension of 10.050 Å × 10.091 Å × 14.114 Å. Our calculations show that NiFe *fcc* unit cell with lattice constant $a = b = c = 3.553$ or 3.582 Å is slightly higher in energy (0.10 and 0.12 kcal/mol, respectively) than the one we employed in the calculations with

$a = c \neq b$. While it is not uncommon that surface reconstruction may occur on bimetallic clusters, the Ni—Fe system is one in which surface segregation is less favored. For example, Ruban et al. [23] have shown that the surface segregation energies of NiFe alloys are unfavorable; positive energies of 0.05–0.3 eV suggest antisegregation. In addition, our own calculations show that formation of islands of a single component on the same plane (i.e., Ni or Fe patches in the parallel direction) is also thermodynamically unfavorable. The energy cost is 0.39 kcal/mol per surface atom for the formation of islands. Therefore, a uniform bulk alloy model is a good representation of the bimetallic clusters, experimentally verified by XRD. In fact, the same model has been employed in recent DFT studies [24].

The adsorption energy (E_{ads}) in this work is defined as $E_{ads} = E_{(al/slab)} - E_{slab} - E_{(al)}$, where $E_{(al/slab)}$, E_{slab}, and $E_{(al)}$ are the total energy of furfural/slab, clean surface, and gas-phase furfural in a supercell.

3. Results

3.1. Catalyst characterization

The XRD patterns of monometallic (Ni/SiO_2 and Fe/SiO_2) and bimetallic (various Ni—Fe/SiO_2) samples, pretreated in H_2 at 450 °C for 1 h, are shown in Fig. 1. No diffraction peaks due to the SiO_2 support were observed. In agreement with previous observations [25], the Ni(1 1 1) and Fe(1 1 0) peaks for the monometallic samples were observed at $2\theta = 44.41°$ and 44.64°, respectively. The bimetallic Ni—Fe/SiO_2 samples exhibited a single peak in this region, and this gradually shifted from the position of pure Ni (44.41°) to smaller angles as the Fe content increased. This shift gives clear evidence for the formation of Ni—Fe solid solution alloys with fcc structure [25]. The absence of any intensity near 44.64° suggests that no unalloyed Fe is present in significant amounts (i.e., detectable by XRD). The lattice constants of Ni and Ni—Fe alloys were estimated from the position of the XRD peaks assuming a cubic symmetry for the crystal structure as shown in Table 1. The lattice constant of Ni is 3.530 Å, which is close to the value obtained from DFT calculation (3.522 Å). Increasingly larger lattice constants (3.542–3.584 Å) were obtained for the Ni—Fe bimetallic samples, in agreement with the DFT calculations and previous reports [26].

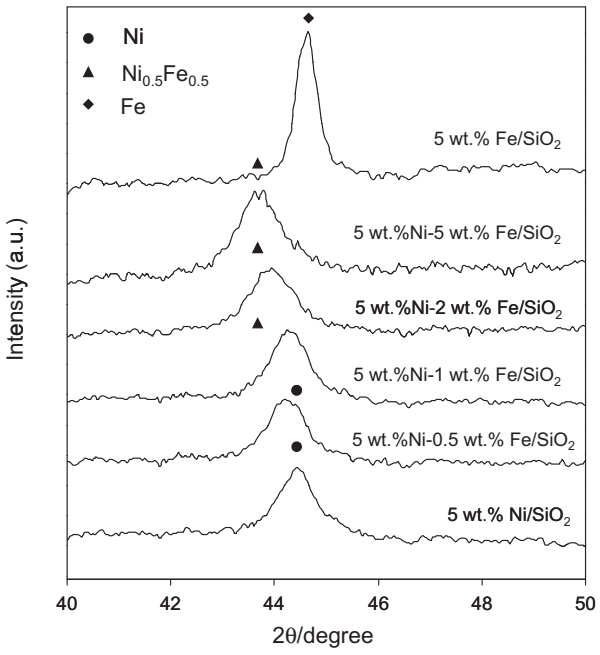

Fig. 1. XRD patterns of monometallic Ni, Fe, and bimetallic Ni—Fe catalysts reduced at 450 °Cfor1 h.

The average particle sizes for Ni and Ni—Fe alloy particles were estimated from the XRD peak broadening, using the Scherrer equation. The values estimated by this method are in the range 10–12 nm for the monometallic Ni and Ni—Fe bimetallic samples. These results agree with those estimated from TEM (see Fig. 2) in the sense that there are no significant size differences between monometallic Ni and Ni—Fe bimetallic particles. By contrast, the monometallic Fe sample has much larger particles than those of

Table 1
Physical properties of catalysts.

Silica-supported catalysts	Metals loading (mmol g_{cat}^{-1})		H_2 consumption from TPR (mmol g_{cat}^{-1})	Diameter (nm)		Lattice constant (Å)			BET (m^2/g)
	Ni	Fe		TEM	XRD	XRD	DFT	Std.	
5 wt.%Ni	0.85	0.00	1.01	16.8	11.2	3.530	3.52	3.52	126
5 wt.%Ni–0.5 wt.%Fe	0.85	0.09	1.16	16.9	11.9	3.542	–	–	130
5 wt.%Ni–1 wt.%Fe	0.85	0.18	1.27	16.7	11.9	3.534	–	–	118
5 wt.%Ni–2 wt.%Fe	0.85	0.36	1.48	17.1	10.0	3.567	–	–	130
5 wt.%Ni–5 wt.%Fe	0.85	0.90	2.20	15.7	10.0	3.584	3.55[a]	3.58[a]	115
5wt.%Fe	0.00	0.90	–	23.4	19.1	2.868	–	2.87	128

[a] $Ni_{0.5}Fe_{0.5}$.

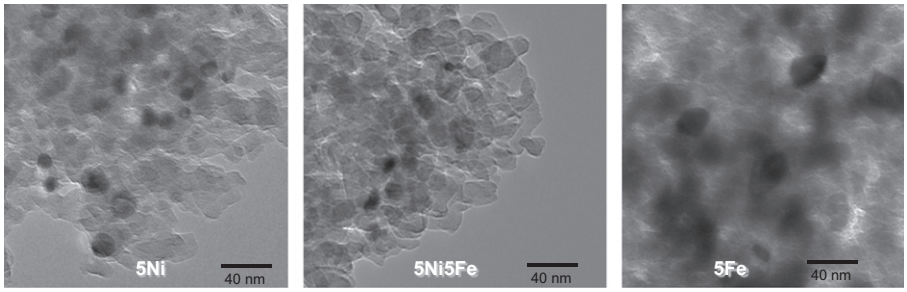

Fig. 2. TEM image of 5 wt.%Ni/SiO_2, 5 wt.%Ni–5 wt.%Fe/SiO_2, and 5 wt.%Fe/SiO_2 catalysts after H_2 pretreatment at 450 °C for 1 h.

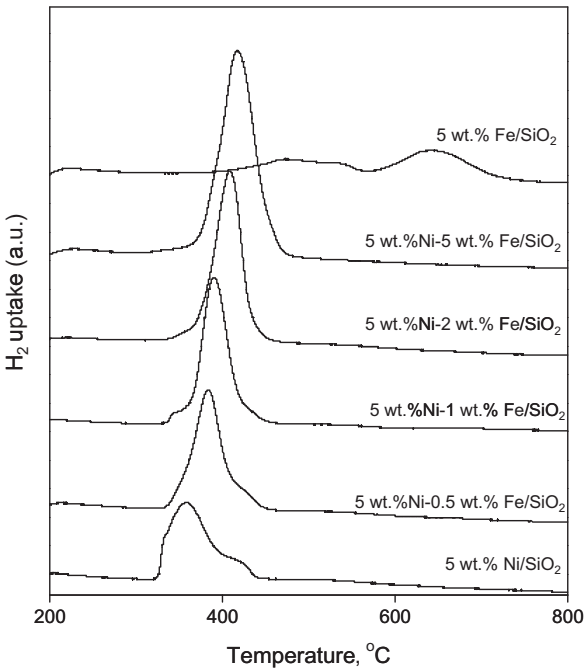

Fig. 3. Temperature programmed reduction (TPR) of monometallic Ni, Fe, and bimetallic Ni—Fe catalysts.

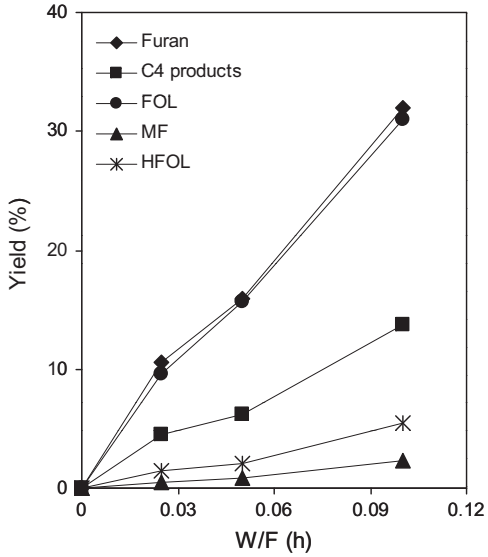

Fig. 4. Product distribution from the reaction of furfural over a monometallic 5 wt.%Ni/SiO_2 catalyst, at 210 °C, H/Feed ratio = 25, pressure = 1 atm.

Ni or Ni—Fe samples, as shown by both XRD (d = 19.1 nm) and TEM (23.4 nm). This difference also supports the conclusion that the bimetallic samples do not contain significant amounts of unalloyed Fe, which would tend to form larger particles.

The large extent of alloy formation is further demonstrated by TPR. As shown in Fig. 3, the reduction profile for the monometallic Ni catalyst displays a main reduction peak at 365 °C with shoulder peaks at lower and higher temperatures (336 and 425 °C, respectively). According to previous studies [27,28], the first peak is the result of an endothermic phase transition occurring simultaneously with a partial reduction of the NiO. The main peak is attributed to the reduction of NiO to Ni metal [29]. The third peak at higher temperatures could be due to the reduction of small nickel oxide crystallites strongly attached to the support, even forming Ni silicate species (nickel hydroxysilicates, antigorite, or montmorillonite) [30]. The reducibility pattern of unalloyed Fe is very different from that of Ni. As seen in Fig. 3, the broad hydrogen consumption peaks for the reduction of Fe/SiO_2 appeared shifted to much higher temperatures from those of Ni. Similar behavior has been reported for monometallic Fe catalysts in previous studies [31]. The first broad peak ranging from 410 to 570 °C has been ascribed to the reduction of α-Fe_2O_3 into α-Fe_3O_4. The second broad peak ranging from 590 to 730 °C with the maximum at 650 °C is typically attributed to the reduction of iron oxides to α-Fe. In sharp contrast to the monometallic Fe sample, the TPR profiles of the Ni—Fe samples do not show any consumption on the high temperature range, which is typical of unalloyed Fe. Instead, as shown in Fig. 3, the addition of Fe only causes a gradual shift to higher reduction temperatures relative to that of pure Ni, in agreement with previous studies [26,32].

In addition to the consistent trend in peak position, the H_2 uptake linearly increased with increasing Fe loading in the bimetallic catalysts (see Table 1). Since the Ni loading was kept constant at 0.85 mmol/g, this proportional increase in H_2 uptake with Fe loading clearly demonstrates the reduction of Fe. The unalloyed Fe is not able to get reduced by itself below 500 °C, as previously reported [33]. Therefore, the almost complete reduction of Fe observed in the bimetallic catalysts demonstrates a close interaction with Ni, consistent with the formation of an alloy.

3.2. Conversion of furfural over monometallic Ni catalyst

The product distribution obtained over the Ni/SiO_2 catalyst at 210 °C is shown in Fig. 4. The most abundant products at this temperature are furfuryl alcohol (FOL, yield = 31% at 0.1 h^{-1}) and furan (yield = 32% at 0.1 h^{-1}), which as shown in Scheme 1, derive from the hydrogenation and decarbonylation reactions, respectively. The next abundant products are those lumped together as C_4 products (yield = 14% at 0.1 h^{-1}), which include butanal, butanol, and butane. The C_4 products derive from the ring-opening reaction via C—O hydrogenolysis of the furan ring (i.e. C2—O2, see

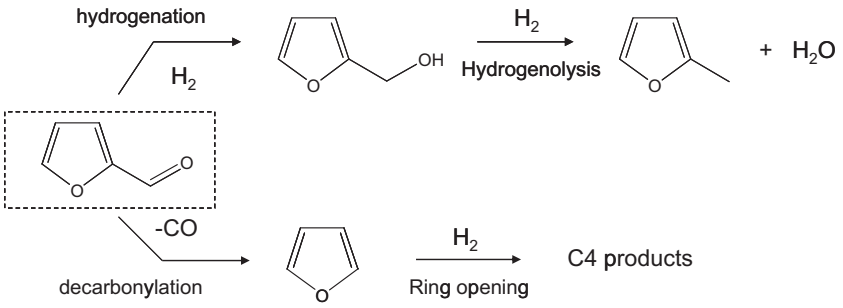

Scheme 1. Reaction pathways for furfural conversion.

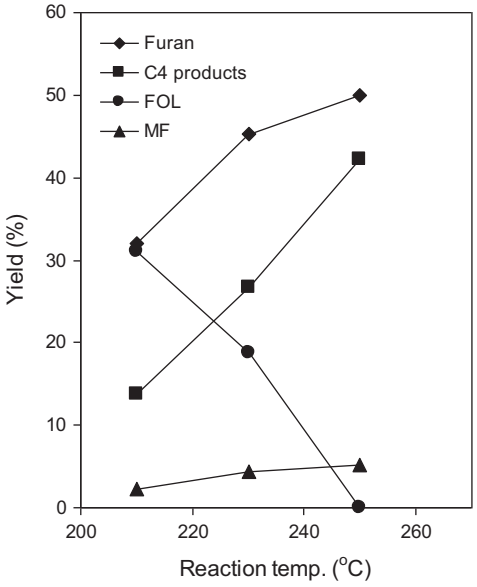

Fig. 5. Yield of products from the reaction of furfural over a monometallic 5 wt.%Ni/SiO_2 catalyst as a function of temperature. Reaction conditions: W/F = 0.1 h, H_2/Feed ratio = 25, pressure = 1 atm.

Fig. 11a for the assignment of each C, O, and H atom), a typical reaction characteristic of Ni catalysts [14,34]. Interestingly, no C_5 products were observed, indicating that the C_4 products mostly derive from furan, rather than from furfural or furfuryl alcohol.

Finally, 2-methylfuran (2MF) produced as a secondary product by the C—O hydrogenolysis of furfuryl alcohol (i.e. C1—O1) is only observed in measurable amounts at high W/F (yield <2% at 0.1 h^{-1}). Similarly, tetrahydrofurfuryl alcohol (HFOL), resulting from hydrogenation of the furanyl ring of furfuryl alcohol, is only observed in significant amounts at high W/F (yield = 5% at 0.1 h^{-1}).

As shown in Fig. 5, a remarkable change in product distribution is observed as the reaction temperature increases. While the yields of furan and its secondary ring-opening C_4 products increase with temperature, furfuryl alcohol rapidly decreases, becoming insignificant near 250 °C. It is clear that decarbonylation and hydrogenation are two parallel routes not strongly dependent on conversion but strongly depend on reaction temperature and type of metals [16,35].

Finally, it is important to note that on the monometallic Ni catalyst, the increase in yield of 2-methylfuran with temperature is much less pronounced than that of the other products, reaching only ~12% at 250 °C.

Table 2
Conversion and yield of products from the reaction of furfural over 5 wt.%Ni/SiO_2 and 5 wt.%Ni–2 wt.%Fe/SiO_2 catalysts.

Catalysts	5 wt.%Ni/SiO_2	5 wt.%Ni–2 wt.%Fe/SiO_2		
W/F (h)	0.025	0.025	0.05	0.1
Conversion (%)	50.9	28.2	51.1	96.3
Furan	23.1	3.8	5.9	12.1
FOL	7.2	5.0	6.4	9.5
MF	1.4	5.0	16.8	39.1
C_4 products	18.1	12.4	19.9	27.6
POL	–	1.0	2.1	7.9

Reaction condition: temp. = 250 °C, H_2/Feed ratio = 25, pressure = 1 atm.

3.3. Conversion of furfural (FAL) over Ni—Fe bimetallic catalysts

A comparison of the conversion levels and product distributions obtained at 250 °C over monometallic 5 wt.%Ni/SiO_2 and bimetallic 5 wt.%Ni–2 wt.%Fe/SiO_2 catalysts at various space times (W/F) is shown in Table 2. The first difference observed is in the level of conversion obtained over the two catalysts under the same reaction conditions. For example, at the same temperature and at W/F = 0.025 h, the overall furfural conversion on the bimetallic catalyst (i.e., 28.2%) was about half of that obtained on the monometallic Ni catalyst (i.e., 50.9%).

In addition, interesting differences in product distribution are observed when comparing the two catalysts. Specifically, comparing them at the same level of conversion (~50%), a clear enhancement in the yield of 2-methylfuran is observed over the bimetallic catalyst. At the same time, the yield of furan greatly decreases on this catalyst. Furthermore, as opposed to the case of monometallic Ni catalyst that did not make any C5 products, the Ni—Fe catalyst produced pentanol (POL) in significant amounts, particularly at high W/F.

It appears that pentanol is formed in a secondary ring-opening reaction of the furanyl ring of 2-methylfuran, which is not

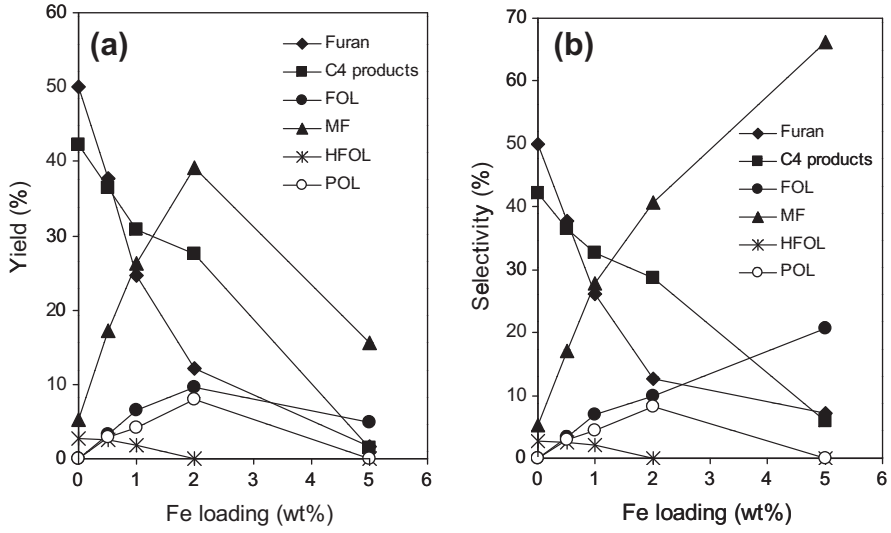

Fig. 6. (a) Yield and (b) selectivity of products from the reaction of furfural over bimetallic Ni—Fe catalysts as a function of Fe loading. Reaction conditions: temp. = 250 °C, W/F = 0.1 h, H_2/Feed ratio = 25, pressure = 1 atm.

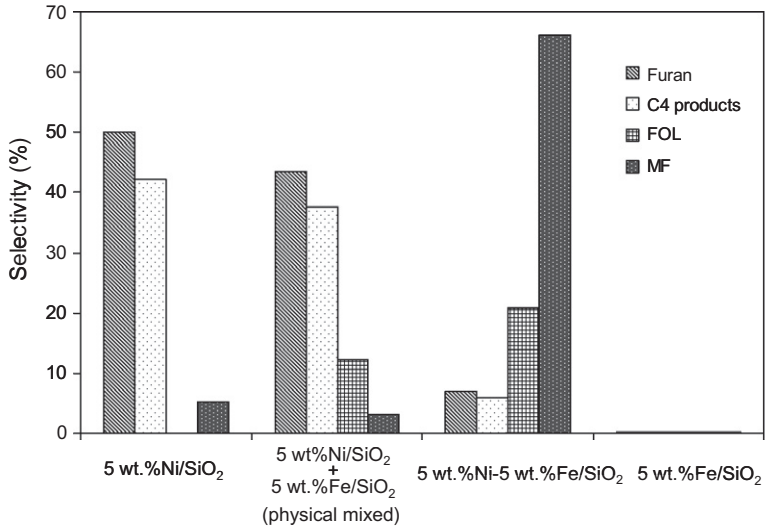

Fig. 7. Product distribution from furfural conversion over various types of catalysts. Reaction conditions: temp. = 250 °C, W/F = 0.1 h, H_2/Feed ratio = 25, pressure = 1 atm.

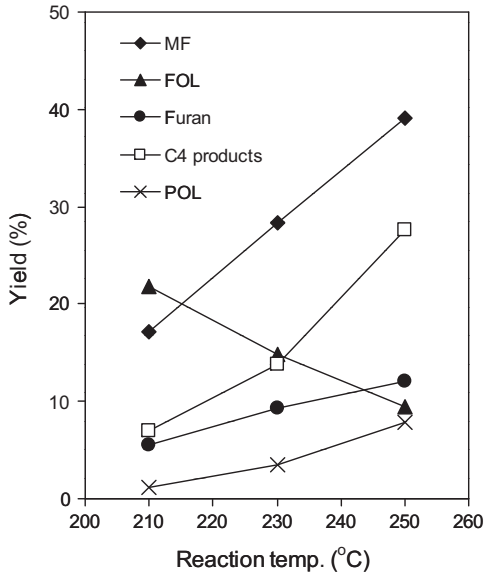

Fig. 8. Product distribution as a function of temperature from the reaction of furfural over 5 wt.%Ni–2 wt.%Fe/SiO_2. Reaction conditions: temp. = 250 °C, W/F = 0.1 h, H_2/Feed ratio = 25, pressure = 1 atm.

significantly formed over the monometallic Ni catalyst. It is also interesting to note that the yield of C_4 products also increased by the addition of Fe, even though the yield of furan was drastically reduced. Since methane was not observed in the products, the C_4 products do not result from the C_5 products. Therefore, it can be concluded that the addition of Fe not only promotes the ring-opening reaction of 2-methylfuran but also of furan.

The effect of Fe loading in the bimetallic catalysts on product distribution is summarized in Fig. 6. It is clear that the addition of Fe on bimetallic catalysts has both a promoting and a suppressing effect on product yield and selectivity. That is, the yield of 2-methylfuran first increases with increasing Fe content to a maximum value at 2%Fe but then decreases, while the selectivity toward 2-methylfuran keeps increasing at all Fe contents. In contrast, the yield and selectivity of furan and C_4 products continuously decrease with Fe loading. It should be noted that, under the present conditions, the monometallic Fe/SiO_2 exhibited no activity for furfural conversion.

To show that the enhanced rate in production of 2-methylfuran at low Fe loadings catalysts is due to a direct interaction between Fe and Ni, a physical mixture of monometallic 5 wt.%Ni/SiO_2 and 5 wt.%Fe/SiO_2 was tested and the results are compared in Fig. 7. They confirm that the product distribution and conversion level are almost the same as those of pure 5 wt.%Ni/SiO_2. That is, furan and its related C_4 products are dominant and the production of 2-methylfuran is very small. By contrast, on the bimetallic 5 wt.%Ni–5 wt.%Fe/SiO_2 catalyst, 2-methylfuran is the main product. Therefore, it is clear that the change in products selectivity of Ni catalyst observed in our experiments is due to the formation of Ni—Fe bimetallic alloys, which have been undoubtedly identified by physicochemical techniques.

The effect of reaction temperature on product distribution over the bimetallic catalyst can be analyzed in Fig. 8. The results show that while furfuryl alcohol and 2-methylfuran are the main products at low temperatures (210°), the yield of 2-methylfuran significantly increases as a function of temperature and it becomes the main product at high temperatures (250 °C). In addition to 2-methylfuran, the ring-opening products from furan and 2-methylfuran also increased with temperature. In contrast to 5 wt.%Ni/SiO_2 catalyst in which furan was the main product at 250 °C, less than 10% yield of furan was observed on the bimetallic 5 wt.%Ni–2 wt.%Fe/SiO_2 catalyst at the same temperature. Again, this result indicates that the presence of Ni—Fe alloys suppresses the decarbonylation activity while it promotes C1—O1 hydrogenolysis reactions, for both the cleavage of the carbonyl group and the opening of the ring. The fact that hydrogenation to furfuryl alcohol was dominant at low temperatures while C1—O1 hydrogenolysis dominated at high temperatures is due to the higher activation of the latter.

Based on the TPR of the Ni—Fe alloys, we conducted the pre-reduction at 450 °C before conducting the reaction in the 200–250 °C temperature range. That is, the alloy is fully reduced before the reaction starts. One could question whether the NiFe alloy remains reduced under reaction conditions. While the reaction conditions are very reducing (H_2/Furfural ratio = 25), water is produced via hydrogenolysis. However, the interaction of water with Ni and Ni—Fe is relatively weak. Our DFT calculations for adsorption of an H_2O molecule on Ni(1 1 1) and NiFe(1 1 1) surfaces show binding energies of −6.6 to −8.4 kcal/mol, respectively, which indicate that, under reaction conditions, H_2O should readily

Table 3
Furfural conversion over various types of reaction conditions.

$T_{reduction}$ (°C)	Pre-reaction steps	Conversion (%)	Yield (%)				
			Furan	C4 products	MF	FOL	POL
450	–	96	12	28	39	10	8
450	Pass H_2 through sat. water at 5 °C[a]	83	10	28	33	5	6
450	Flow 5% O_2/He[a]	38	4	12	13	7	2
250	–	13	1	2	2	7	0

Condition: Catalyst: 5 wt.%Ni–2 wt.%Fe/SiO_2, Temp. = 250 °C, W/F = 0.1 h, H_2/Feed ratio = 25, pressure = 1 atm.
[a] For 10 min.

desorb from the metals upon formation. Moreover, previous studies [36,37] have shown that H_2O dissociation on Ni(1 1 1) has a high activation barrier (22.4 kcal/mol) compared to that of H_2 dissociation (~0 on Ni(1 1 1)).

To determine how an oxidized surface would behave, we compared the conversion and product distribution of furfural over the 5 wt.%Ni–2 wt.%Fe/SiO_2 catalyst with the following pre-reaction steps:

(a) pre-oxidation with water vapor at 250 °C; after the initial reduction at 450 °C,
(b) pre-oxidation in 5% O_2 at 250 °C; after the initial reduction at 450 °C,
(c) reduction at 250 °C.

As shown in Table 3, a continuous decrease in activity is observed with increasing extent of oxidation severity. In fact, it is expected that the more oxidized is the surface, the lower the extent of hydrogenolysis (i.e. lower MF yield) will be. That is, the fully reduced alloy, kept under the reducing conditions, is the one with the highest hydrogenolysis activity.

3.4. Conversion of furfuryl alcohol (FOL) over Ni—Fe bimetallic catalysts

To further investigate the reaction pathways of oxygenates over the Ni—Fe bimetallic catalysts and shed more light on the results obtained with furfural, we conducted reaction measurements using additional oxygenated molecules on the same catalyst series. We first chose to study the conversion of furfuryl alcohol under the same reaction conditions as those used with furfural to determine whether the hydrogenation of the carbonyl group makes hydrogenolysis easier. If that is the case, C1—O1 hydrogenolysis could occur as a secondary reaction with the alcohol acting as an intermediate (see Scheme 1).

Having furfuryl alcohol as the feed, the main primary products on pure Ni are furan and 2-methylfuran. As the Fe loading increases, the yield of furan decreased while 2-methylfuran increased, as with the furfural feed. The yield of pentanol (POL), which derives from C2—O2 hydrogenolysis of 2-methylfuran, also increased significantly when Fe was incorporated.

While similar distribution of products are obtained with furfuryl alcohol and furfural feeds, the most important difference is the high activity for 2-methylfuran formation from furfuryl alcohol compared to that from furfural, as shown in Fig. 9b as a function of Fe loading in the Ni—Fe bimetallic catalysts. A significantly higher yield of 2-methylfuran is obtained from furfuryl alcohol than from furfural in everyone of the catalysts, but the difference becomes more pronounced as the Fe/Ni ratio increases.

3.5. Conversion of tetrahydrofurfuryl alcohol (HFOL) over Ni—Fe bimetallic catalysts

It is important to determine whether the much faster deoxygenation observed with the alcohol compared to that with the aldehyde is due to enhanced C1—O1 hydrogenolysis reaction or a combination of partial hydrogenation/dehydration. One could speculate that instead of the direct activation of the C—O bond via a di-sigma intermediate mentioned above, a partial hydrogenation of the furanyl ring, followed by dehydration of the alcohol, may operate on these catalysts leading to 2-methylfuran. Therefore, to eliminate this possibility, we measured the conversion of tetrahydrofurfuryl alcohol (HFOL) over the same 5 wt.%Ni–2 wt.%Fe/SiO_2 catalyst, under the same reaction conditions as those used with furfuryl alcohol and furfural. Contrary to the reaction with furfural and particularly with furfuryl alcohol for which a high

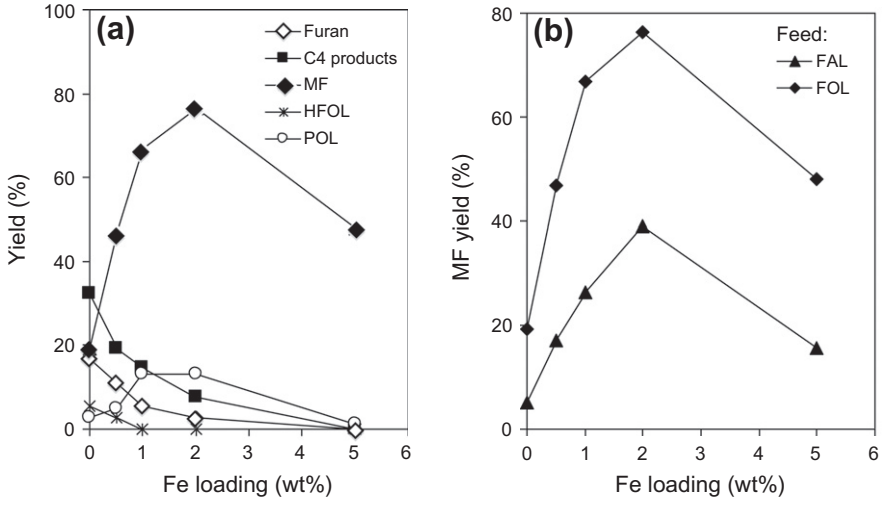

Fig. 9. (a) Yield of products from the reaction of furfuryl alcohol over Ni—Fe bimetallic catalysts as a function of Fe loading. (b) Comparison of methylfuran yield from furfural and furfuryl alcohol feeds. Reaction conditions: temp. = 250 °C, W/F = 0.1 h, H_2/Feed ratio = 25, pressure = 1 atm.

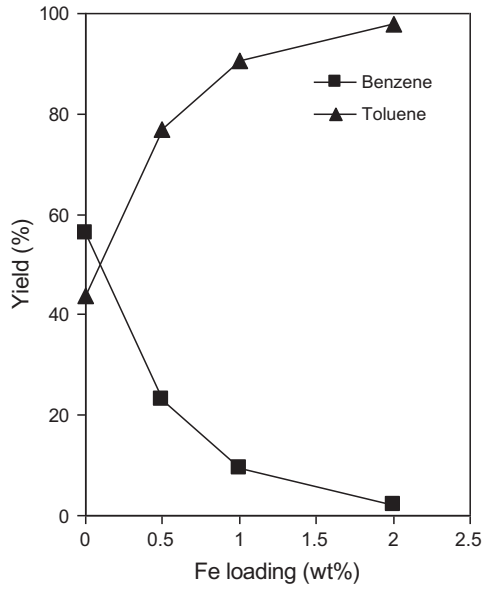

Fig. 10. Yield of products from the reaction of benzyl alcohol over Ni—Fe bimetallic catalysts as a function of Fe loading. Reaction conditions: temp. = 250 °C, W/F = 0.1 h, H_2/Feed ratio = 25, pressure = 1 atm.

yield of 2-methylfuran was observed (~40%), with the fully saturated tetrahydrofurfuryl alcohol, the yield of 2-methyltetrahydrofuran was very low (~1.5%) and 2-methylfuran was not observed. The much lower reactivity of tetrahydrofurfuryl alcohol demonstrates that dehydration is not an important reaction path on these catalysts. By contrast, the strong interaction of the furanyl ring with the metal surface seems to play an important role in the C—O hydrogenolysis reaction. In fact, it is generally known that furan has a strong interaction with the surface of Group VIII metals due to the interaction of the p bonds of the ring with the d orbitals of the metal [38,39].

3.6. Conversion of benzyl alcohol (BZOL) over Ni—Fe bimetallic catalysts

To investigate whether the presence of an aromatic ring in the molecule plays a similar role in reactivity as that of the furanyl ring in the conversion of the oxygenated group, we investigated the conversion of benzyl alcohol over the same catalysts series as that used for the furanyl compounds. To determine to what extent the relative decarbonylation/hydrogenolysis reaction rates can be modified by the addition of Fe, we evaluated the formation of benzene and toluene as direct products of decarbonylation and hydrogenolysis, respectively. The major difference with the products from furfural and furfuryl alcohol was the lack of ring-opening products, which indicate that the aromatic ring remains unperturbed during the reaction.

The most important similarity was the enhancement of hydrogenolysis and reduction in decarbonylation activity as the Fe/Ni ratio increased. Fig. 10 clearly shows that as the Fe content increases in the bimetallic catalysts, the product distribution drastically changes from almost 60% benzene on pure Ni to almost 100% toluene on the 5 wt.%Ni–2 wt.%Fe/SiO_2 catalyst.

3.7. Adsorption of furfural and furfuryl alcohol on Ni(1 1 1) and NiFe(1 1 1) surfaces

Density Functional Theory (DFT) calculations have been made to investigate geometries and relative stabilities of the possible furfural species adsorbed on the surface of pure Ni(1 1 1) and a bimetallic NiFe(1 1 1) alloy. We have also evaluated the differences observed on heats of adsorption and bond lengths when furfuryl alcohol is considered as an adsorbate. These calculations have helped us to interpret the changes observed in product selectivities from monometallic Ni to Ni—Fe bimetallic catalysts and to elucidate possible reaction pathways.

First, the optimized structures of furfural in the gas phase and adsorbed on the Ni(1 1 1) and NiFe(1 1 1) surfaces in an upright and planar configuration are illustrated in Figs. 11 and 12 respectively. The corresponding adsorption energies (E_{ads}) and bond lengths of a planar configuration are summarized in Table 4. It can be seen that for both surfaces under the conditions investigated (i.e., low furfural coverage), the upright configuration with only the carbonyl O sitting on the metal surface is less favored than the planar adsorption configuration. For example, the adsorption energies on for upright and planar configurations Ni(1 1 1) are −8.9 and −15.6 kcal/mol, respectively. The optimized geometries of planar configuration show that the carbonyl group (C=O) adsorbed on a bridge site and the furanyl ring plane sitting parallel to the surface across two 3-fold hollow sites on.

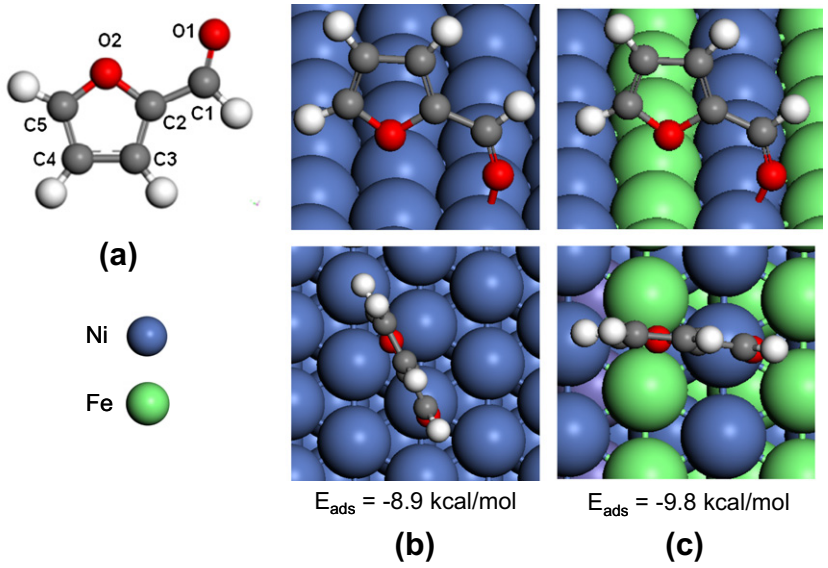

Fig. 11. Optimized furfural structures of (a) gas phase, (b) adsorbed on Ni(1 1 1), and (c) adsorbed on NiFe(1 1 1) surfaces with an upright configuration.

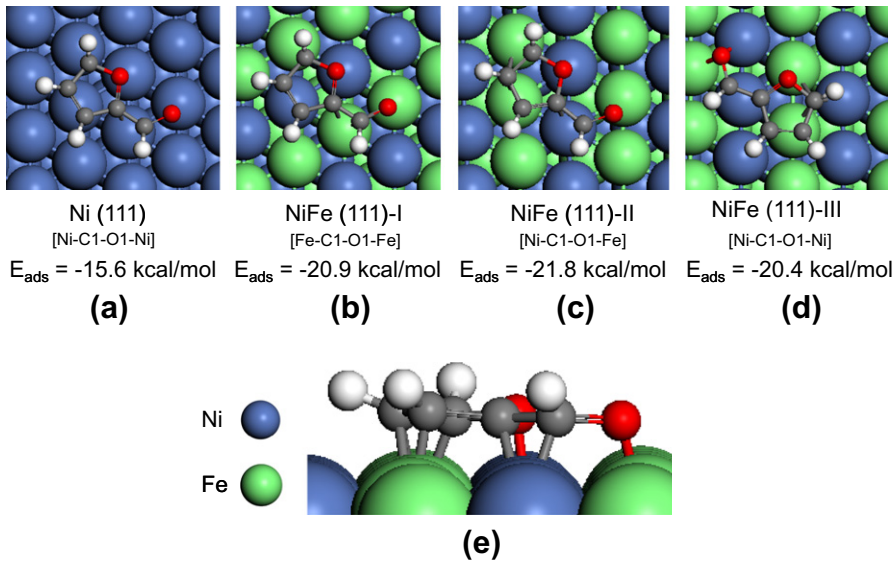

Fig. 12. Optimized structures of furfural adsorbed on (a) Ni(1 1 1) surface and NiFe(1 1 1) surface (b–d), and side view (e) with a planar configuration.

As shown in Table 4 for the more stable planar configurations, the bond lengths for the C—C bonds in the furanyl ring increase on both surfaces, suggesting a slight enlargement of the ring, resulting from the interaction with the surface. In addition, a more significant increase in bond length upon adsorption is observed for the C—O bond of the carbonyl group. It is well known that aldehydes on Group VIII metals adsorb in an η^2-(C,O) configuration with both C and O atoms linked to the metal surface [16,42]. Therefore, an increased C—O bond length is expected on the adsorbed furfural species on Ni. On the other hand, of greater interest is the small but consistent increase in C—O bond length observed on the Ni—Fe bimetallic surfaces compared to the pure Ni surface. This difference not only shows that the presence of Fe does not inhibit the formation of the η^2-(C,O) configuration, but rather it enhances the interaction with the carbonyl group. We recently described an opposite behavior working with the Pd—Cu bimetallic system [16]. In that case, experimental and theoretical data gave evidence to the inhibition of the formation of η^2-(C,O) when Cu was added to Pd. Addition of Cu generates a strong repulsion to the C atom that favors the formation of η^1-(O) over the η^2-(C,O) species. Previously we had also shown that a similar repulsion occurs between the monometallic Cu(1 1 1) surface and the furanyl ring, due to the overlap of the 3d band of the surface Cu atoms and the aromatic furan ring [7]. As a result, the adsorption of furfural on Cu(1 1 1) is weak and can only occur in the η^1(O)-aldehyde configuration, via the carbonyl O atom.

This is not the case with the addition of Fe to Ni, which causes a significant increase in the resulting furfural adsorption energy (i.e. 15.6 kcal/mol on Ni to 20.4–21.8 kcal/mol on NiFe). Some variations in energy are observed depending on the position of the molecule on the NiFe(1 1 1) surface. Adsorption with the C atom on top of Ni and the O atom on Fe showed the highest energy (NiFe(1 1 1)-II) indicating a strong interaction between the carbonyl O atom and Fe on the surface. This result is consistent with those of acrolein adsorption on Pt and PtFe surfaces [40]. It was concluded that acrolein adsorbs in a parallel configuration on Pt(1 1 1) surface with both double bonds interacting with the surface. When Fe atoms are present in the surface, adsorption geometries including O—Fe interactions become much more stable.

Fig. 13 shows calculated projected-DOS for C1—O1 in the carbonyl group of the adsorbate and two metal atoms of the metal bridge site on which they are bound. For comparison with these electronic structures, the discrete (C1—O1)-2p states for gas-phase furfural and the PDOS for the clean metal surfaces are included in Figs. 13f and e, respectively. In particular, it is observed that the π^*-states of carbonyl C1—O1, which are unoccupied in the gas-phase furfural and centered near 3 eV above the Fermi level, are downshifted below the Fermi level and significantly broadened in the adsorbed state. This shift favors the electron-back donation from the metal 3d-states to the anti-bonding π^*-states of the carbonyl, which is in line with the observed increases in C1—O1 bond length, as reported in Table 4. It is interesting to note the slight differences

Table 4
Comparison of bond lengths (Å) of furfural in gas phase and adsorbed on Ni(1 1 1) and NiFe(1 1 1) surfaces. See Fig. 12 (a–d) for adsorption of furfural in planar configurations and (f) for the assignment of each C, O, and H atom. A comparison is also made with furfuryl alcohol dissociatively adsorbed on the same surfaces (see Fig. 14). Adsorption energies (E_{ads}) in kcal/mol are included.

d	Furfural	Furfural				Furfuryl alcohol	
	Gas phase	Ni(1 1 1)	NiFe(1 1 1) I	NiFe(1 1 1) II	NiFe(1 1 1) III	Ni(1 1 1)	NiFe(1 1 1) II
Cl—Hl	1.120	1.103	1.101	1.100	1.102	1.092	1.094
Cl—Ol	1.229	1.319	1.340	1.347	1.349	1.377	1.433
C1—C2	1.448	1.439	1.425	1.440	1.446	1.420	1.429
C2—C3	1.382	1.440	1.438	1.444	1.448	1.441	1.441
C3—C4	1.419	1.429	1.448	1.443	1.420	1.437	1.451
C4—C5	1.373	1.450	1.455	1.449	1.452	1.451	1.454
C5—O2	1.359	1.465	1.456	1.459	1.476	1.466	1.469
C2—O2	1.378	1.408	1.389	1.403	1.428	1.404	1.399
E_{ads}	kcal/mol	−15.6	−20.9	−21.8	−20.4	−27.6	−27.1

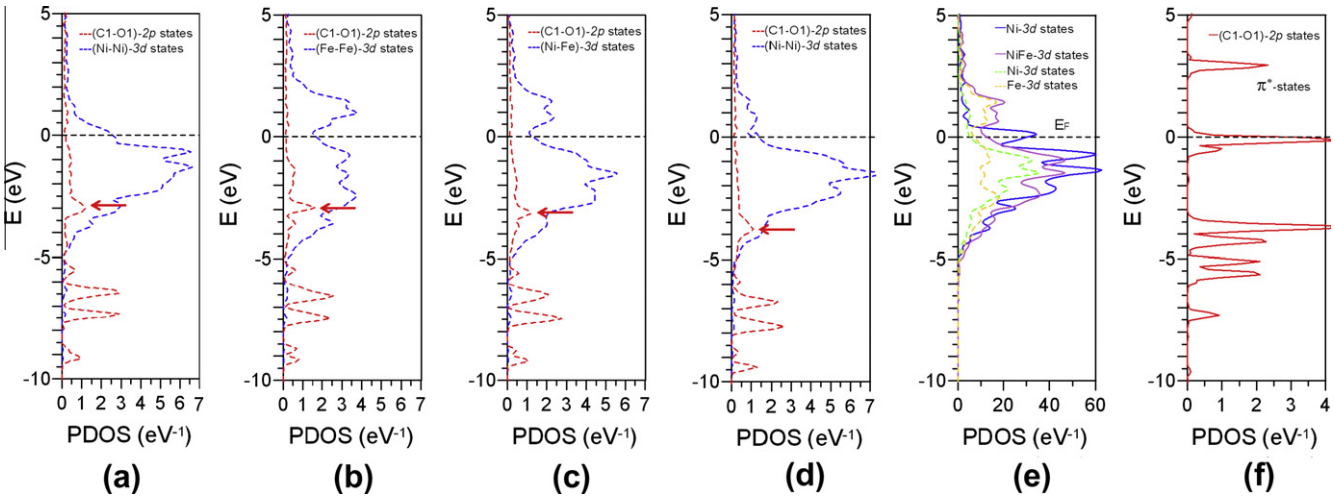

Fig. 13. Calculated PDOS for furfural adsorbed on Ni(1 1 1) and NiFe(1 1 1) surface, corresponding to the adsorption configuration in Fig. 12 (a–d), respectively. PDOS for clean surface (e) and gas-phase furfural (f) also included for comparison.

in the position of this peak below the Fermi level for the various adsorbate/metal species. In particular, for Ni and NiFe in the configuration I, it appears around 3.0 eV below the Fermi level, but it shifts to 3.3 and 3.7 eV for configurations II and III, respectively. Indicating that certain configurations on the bimetallic surface may result in a greater extent of back-donation, which may further weaken the C—O bond.

The experimental results indicate that the C—O hydrogenolysis is much faster with furfuryl alcohol than with furfural; so, it is highly possible that the path for formation of 2-methylfuran goes through an alcohol intermediate. Therefore, we have conducted additional DFT calculations on Ni(1 1 1) and bimetallic NiFe(1 1 1) by considering a hydroxyalkyl intermediate ($C_5H_4O(OH)$) that is expected to result from the dissociative adsorption of furfuryl alcohol ($C_5H_5O(OH)$) (see Fig. 14).

As summarized in Table 4, the calculations indicate that on both surfaces, the adsorption strength is significantly enhanced compared to that of furfural. However, the most interesting result is the significant lengthening of the C1—O1 bond on the bimetallic NiFe(1 1 1) surface compared to that on pure Ni(1 1 1) surface (i.e., 1.433 vs. 1.377 Å). This bond lengthening on the bimetallic surface reflects a further weakening of the C—O bond, which is consistent with the higher C—O hydrogenolysis rate observed experimentally.

4. Discussion

The proposed reaction pathways for furfural conversion are summarized in Scheme 1. Furfuryl alcohol and furan are primary products typically observed over Ni-based catalysts [14,41], and they can further convert to 2-methylfuran and ring-opening C_4

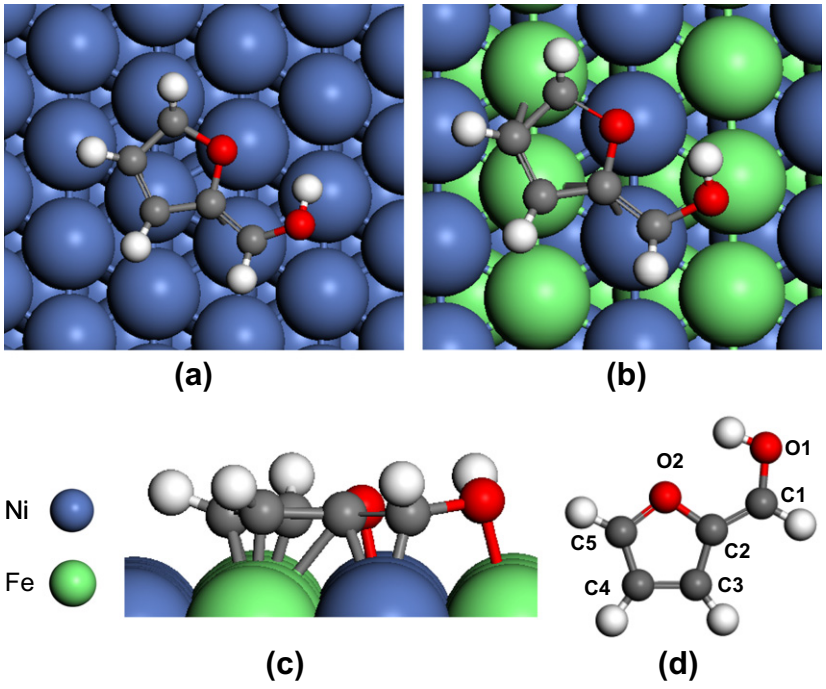

Fig. 14. Optimized structures of furfuryl alcohol dissociatively adsorbed on Ni(1 1 1) surface (a) and NiFe(1 1 1) surface (b). Side view of surface and gas-phase hydroxyalkyl intermediate structures are shown in (c) and (d), respectively.

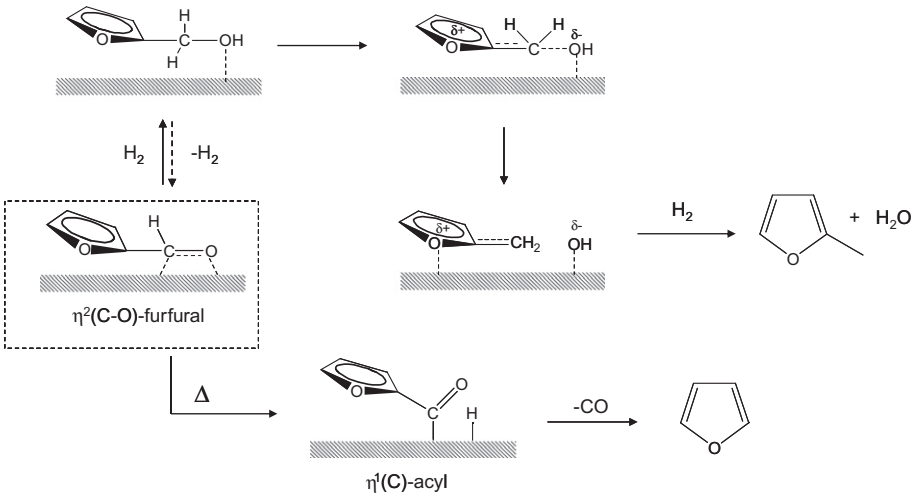

Scheme 2. Possible species on the surface during conversion of furfural.

products, respectively. We have shown here that this product distribution can vary significantly with reaction temperature and the presence of Fe in the bimetallic catalysts.

Our results show that on monometallic Ni catalyst, decarbonylation is favored over hydrogenation, particularly at high reaction temperatures. A behavior that is similar to that of Pd catalysts [14,16]. This behavior can be explained in terms of the stability of the surface species at different temperatures. Spectroscopic results and DFT calculations show that, on group VIII metals, aldehydes tend to adsorb with the carbonyl group parallel to the surface (η^2(C,O)-aldehyde) [42–44]. As summarized in Scheme 2, this configuration favors the hydrogenation of the carbonyl group, yielding furfuryl alcohol, as experimentally observed at low temperature. However, at high temperature, η^2(C,O)-furfural tends to decompose into a more stable acyl species, in which the C atom of the carbonyl remains strongly attached to the surface. This acyl species may in fact be a precursor for the decarbonylation reaction, yielding furan and CO [35]. As shown in Fig. 5, the selectivity to decarbonylation significantly increases as a function of temperature, which is consistent with an activated conversion of η^2(C,O)-furfural into the acyl species that increases decarbonylation while reducing hydrogenation. This observation is in excellent agreement with the HREELS experiments of acetaldehyde adsorbed on clean Pt(1 1 1) [45] which shows that, at low temperatures, an η^2(C,O) surface species was formed, but it was readily decomposed above 330 K, producing an acetyl intermediate that was stable up to 440 K.

In addition to the differences in interaction with the carbonyl group itself, different metals have a different extent of interaction with the furanyl ring. For example, while Cu exerts a repulsion on the ring [7], Group VIII metals tend to interact strongly with aromatic [46] and furanyl rings [16], as well as C=C double bonds [47]. In particular, on Ni surfaces the furanyl ring/metal interaction is so strong that C—O bond in the ring weakens and leads to a significant extent of ring opening (i.e. C2—O2 hydrogenolysis), a reaction that is also favored as temperature increases.

The selectivity to 2-methylfuran is an interesting case. Since, as shown above, the C1—O1 hydrogenolysis occurs mainly after furfural has been hydrogenated to furfuryl alcohol and this product is not favored on pure Ni, particularly at the high temperatures required for C—O hydrogenolysis, very small amounts of 2-methylfuran are produced on monometallic Ni.

This situation is drastically altered when Fe is added to the Ni-based catalysts. First of all, decarbonylation is greatly suppressed on the bimetallic catalysts, which can be again explained in terms of the stability of the surface species. In this case, the DFT calculations suggest that the oxophilic nature of Fe makes the di-bonded η^2(C,O)-furfural more stable than on the pure Ni surface. The longer C1—O1 bond length of the adsorbed η^2(C,O)-furfuryl alcohol indicates that the overall stronger interaction of the C=O group with the Ni—Fe alloy surface results in the weakening of the C1—O1 bond. As a result, it is reasonable to speculate that the formation of acyl intermediate would require a higher energy barrier, which explains the drastic reduction in the rate of decarbonylation observed on the bimetallic catalysts (see Scheme 2).

The enhanced yield of C1—O1 hydrogenolysis products over Ni—Fe bimetallic catalysts from furfuryl alcohol and benzyl alcohol further support this concept. On the monometallic Ni catalysts, furan and benzene are the main products resulting from decarbonylation of furfuryl alcohol and benzyl alcohol, respectively. These products greatly decrease on the bimetallic catalysts, which mainly yield C1—O1 hydrogenolysis products due to the stabilization of the η^2(C,O) intermediate compared to the acyl intermediate.

5. Conclusion

The conversion of furfural on pure Ni/SiO_2 catalysts yields primarily decarbonylation products due to the favorable formation of acyl species, which can readily decompose into furan and CO at high temperature. In addition, furan can further react to ring-opening products due to the strong interaction of the furan ring with Ni surfaces. In contrast, furfuryl alcohol is produced in significant low amounts, which in turn results in low formation of 2-methylfuran.

By adding Fe to the catalysts, Ni—Fe alloys are formed, as evidenced by TPR and XRD. The product selectivity is drastically shifted to 2-methylfuran while decarbonylation products and their derivatives are suppressed. This reduction in decarbonylation can be attributed to an increase of the stability of η^2(C,O)-surface species. The increase in the interaction of the carbonyl O with surfaces through Fe—O interaction hinders the formation of acly species, which is responsible for decarbonylation. In addition, the C—O hydrogenolysis of the adsorbed furfuryl alcohol is improved by this interaction.

Acknowledgments

This work was partially supported by the National Science Foundation EPSCOR (Grant 0814361) and the Department of

Energy (Grant DE-FG36GO88064). The authors are grateful to Dr. Tawan Sooknoi for very useful discussions. The XRD analysis was conducted with the assistance of Dr. Rolf E. Jentoft and his encouragement is gratefully acknowledged.

References

[1] R. He, X.P. Ye, B.C. English, J.A. Satrio, Bioresour. Technol. 100 (2009) 535.
[2] D.C. Elliott, T.R. Hart, Energy Fuels 23 (2009) 631.
[3] J.N. Chheda, J.A. Dumesic, Catal. Today 123 (2007) 59.
[4] R.M. West, E.L. Kunkes, D.A. Simonetti, J.A. Dumesic, Catal. Today 147 (2009) 115.
[5] G.W. Huber, J.A. Dumesic, Catal. Today 111 (2006) 119.
[6] L. Faba, E. Diaz, S. Ordonez, Catal. Today 164 (2011) 451.
[7] S. Sitthisa, T. Sooknoi, Y. Ma, P.B. Balbuena, D.E. Resasco, J. Catal. 277 (2011) 1.
[8] G. Seo, H. Chon, J. Catal. 67 (1981) 424.
[9] R. Rao, A. Dandekar, R.T.K. Baker, M.A. Vannice, J. Catal. 171 (1997) 406.
[10] B.M. Reddy, G.K. Reddy, K.N. Rao, A. Khan, I. Ganesh, J. Mol. Catal. A 265 (2007) 276.
[11] H. Li, H. Luo, L. Zhuang, W. Dai, M. Qiao, J. Mol. Catal. A 203 (2003) 267.
[12] B. Liaw, S. Chiang, S. Chen, Y. Chen, Appl. Catal. A 346 (2008) 179.
[13] J. Kijeński, P. Winiarek, T. Paryjczak, A. Lewicki, A. Mikołajska, Appl. Catal. A 233 (2002) 171.
[14] S. Sitthisa, D.E. Resasco, Catal. Lett. 141 (2011) 784.
[15] Y. Roman-Leshkov, C.J. Barrett, Z.Y. Liu, J.A. Dumesic, Nat. Lett. 447 (2007) 982.
[16] S. Sitthisa, T. Pham, T. Prasomsri, T. Sooknoi, R.G. Mallinson, D.E. Resasco, J. Catal. 280 (2011) 17.
[17] G. Kresse, J. Hafner, Phys. Rev. B 48 (1993) 13115.
[18] G. Kresse, J. Furthmuller, Phys. Rev. B 54 (1996) 11169.
[19] J.P. Perdew, K. Burke, M. Ernzerhof, Phys. Rev. Lett. 77 (1996) 3865.
[20] P.E. Blochl, Phys. Rev. B 50 (1994) 17953.
[21] G. Kresse, D. Joubert, Phys. Rev. B 59 (1999) 1758.
[22] M. Hayase, M. Shiga, Y. Nakamura, J. Phys. Soc. Jpn. 34 (1973) 925.
[23] A.V. Ruban, H.L. Skriver, J.K. Norskov, Phys. Rev. B 59 (1999) 15990.
[24] C. Fan, X.G. Zhou, D. Chen, H.Y. Cheng, Y.A. Zhu, J. Chem. Phys. 134 (2011) 134704.
[25] L. Wang, D. Li, M. Koike, S. Koso, Y. Nakagawa, Y. Xu, K. Tomishige, Appl. Catal. A: Gen. 392 (2011) 248.
[26] T. Ishihara, K. Eguchi, H. Arai, Appl. Catal. 30 (1987) 225.
[27] Y. Colombo, F. Gazzarini, G. Lanzavecchia, Mater. Sci. Eng. 2 (1967) 125.
[28] J. Szekely, C.I. Lin, H.Y. Sohn, Chem. Eng. Sci. 28 (1973) 1975.
[29] M.A. Ermakova, D.Y. Ermakov, Catal. Today 77 (2002) 225.
[30] B. Mile, D. Stirling, M.A. Zammitta, A. Lovell, M. Webb, J. Mol. Catal. 62 (1990) 179.
[31] H. Jung, W.J. Thomson, J. Catal. 128 (1991) 218.
[32] A.L. Kustov, A.M. Frey, K.E. Larsen, T. Johannessen, J.K. Norskov, C.H. Christensen, Appl. Catal. A: Gen. 320 (2007) 98.
[33] E.E. Unmuth, L.H. Schwartz, J.B. Butt, J. Catal. 61 (1980) 242.
[34] Z. Xinghua, W. Tiejun, M. Longlong, W. Chuangzhi, Fuel 89 (2010) 2697.
[35] R.D. Srivastava, A.K. Guha, J. Catal. 91 (1985) 254.
[36] M. Pozzo, G. Carlini, R. Rosei, D. Alfe, J. Chem. Phys. 126 (2007) 164706.
[37] B.I. Liu, M.A. Lusk, J.F. Ely, J. Phys. Chem. C 113 (2009) 13715.
[38] M.K. Bradley, J. Robinson, D.P. Woodruff, Surf. Sci. 604 (2010) 920.
[39] C.J. Kliewer, C. Aliaga, M. Bieri, W. Huang, C.-K. Tsung, J.B. Wood, K. Komvopoulos, G.A. Somorjai, J. Am. Chem. Soc. 132 (2010) 13088.
[40] R. Hirschl, F. Delbecq, P. Sautet, J. Hafner, J. Catal. 217 (2003) 354.
[41] R.M. Lukes, C.L. Wilson, J. Am. Chem. Soc. 73 (1951) 4790.
[42] M. Mavrikakis, M.A. Barteau, J. Mol. Catal. A: Chem. 131 (1998) 135.
[43] R. Shekhar, R.V. Plank, J.M. Vohs, M.A. Barteau, J. Phys. Chem. B 101 (1997) 7939.
[44] J.L. Davis, M.A. Barteau, J. Am. Chem. Soc. 111 (1989) 1782.
[45] M.A. Henderson, Y. Zhou, J.M. White, J. Am. Chem. Soc. 111 (1989) 1185.
[46] C. Morin, D. Simon, P. Sautet, J. Phys. Chem. B 108 (2004) 12084.
[47] F. Delbecq, P. Sautet, J. Catal. 211 (2002) 398.